Bioactive Materials 19 (2023) 678–689

Contents lists available at ScienceDirect

Bioactive Materials

journal homepage: www.keaipublishing.com/en/journals/bioactive-materials

An immunomodulatory polypeptide hydrogel for osteochondral defect repair

Meng Yang [a,c,1], Zheng-Chu Zhang [b,1], Fu-Zhen Yuan [a,c,1], Rong-Hui Deng [a,c], Xin Yan [a,c], Feng-Biao Mao [d], You-Rong Chen [a,c,***], Hua Lu [b,**], Jia-Kuo Yu [a,c,*]

[a] *Department of Sports Medicine, Beijing Key Laboratory of Sports Injuries, Peking University Third Hospital, Beijing, 100191, China*
[b] *Beijing National Laboratory for Molecular Sciences, Center for Soft Matter Science and Engineering, Key Laboratory of Polymer Chemistry and Physics of Ministry of Education, College of Chemistry and Molecular Engineering, Peking University, Beijing, 100871, People's Republic of China*
[c] *Institute of Sports Medicine of Peking University, Beijing, 100191, China*
[d] *Institute of Medicine Innovation and Research Peking University Third Hospital, Beijing, 100191, China*

ARTICLE INFO

Keywords:
Osteochondral regeneration
Polypeptide hydrogel
Immunoregulation
Foreign-body reaction
Mesenchymal stem cells

ABSTRACT

Osteochondral injury is a common and frequent orthopedic disease that can lead to more serious degenerative joint disease. Tissue engineering is a promising modality for osteochondral repair, but the implanted scaffolds are often immunogenic and can induce unwanted foreign body reaction (FBR). Here, we prepare a polypept(o)ide-based PAA-RGD hydrogel using a novel thiol/thioester dual-functionalized hyperbranched polypeptide P(EG$_3$Glu-*co*-Cys) and maleimide-functionalized polysarcosine under biologically benign conditions. The PAA-RGD hydrogel shows suitable biodegradability, excellent biocompatibility, and low immunogenicity, which together lead to optimal performance for osteochondral repair in New Zealand white rabbits even at the early stage of implantation. Further *in vitro* and *in vivo* mechanistic studies corroborate the immunomodulatory role of the PAA-RGD hydrogel, which induces minimum FBR responses and a high level of polarization of macrophages into the immunosuppressive M2 subtypes. These findings demonstrate the promising potential of the PAA-RGD hydrogel for osteochondral regeneration and highlight the importance of immunomodulation. The results may inspire the development of PAA-based materials for not only osteochondral defect repair but also various other tissue engineering and bio-implantation applications.

1. Introduction

Osteochondral defects are mainly caused by wear out and accidental trauma such as sports injury, which can lead to osteoarthritis and severe joint pain [1]. Because mature articular cartilage has almost no blood supply and limited ability to repair itself, osteochondral defects can be irreversible and permanent if inappropriately treated [2]. Currently, the most commonly used treatments for osteochondral defects include microfracture surgery, and osteochondral allograft transplantation (OCT) [3,4]. However, problems such as irreversible cartilage degeneration, foreign body reaction (FBR), and undesired fibrocartilage rather than hyaline cartilage formation, are frequently observed in the abovementioned methods and limit their surgical effects [5,6].

Recently, tissue engineering scaffolds with composite seed cells, mesenchymal stem cells (MSCs) and chondrocytes for example, have become a promising treatment for osteochondral defects [7]. Hydrogels are widely used in tissue engineering as scaffold materials because of their high-water content and biocompatibility [8–19]. To achieve functional repair, ideally, the scaffolds need to have optimal properties, including suitable degradability, low immunogenicity, and low toxicity [20]. For instance, the degradation rate of the scaffold needs to match the ingrowth rate of new tissue for better extracellular matrix (ECM) deposition [21,22]. Currently, most hydrogels fail to offer satisfactory repairing effect at the early stage, partially due to suboptimal

Peer review under responsibility of KeAi Communications Co., Ltd.
* Corresponding author. Department of Sports Medicine, Beijing Key Laboratory of Sports Injuries, Peking University Third Hospital, Beijing, 100191, China.
** Corresponding author.
*** Corresponding author. Department of Sports Medicine, Beijing Key Laboratory of Sports Injuries, Peking University Third Hospital, Beijing, 100191, China.
E-mail addresses: chenyourong1990@163.com (Y.-R. Chen), chemhualu@pku.edu.cn (H. Lu), yujiakuo@126.com (J.-K. Yu).
[1] These authors contributed equally to this work.

https://doi.org/10.1016/j.bioactmat.2022.05.008
Received 15 March 2022; Received in revised form 30 April 2022; Accepted 4 May 2022

degradation rates [23]. More importantly, as foreign objects, the implanted scaffolds need to be minimally immunogenic to prevent potential FBR [24,25].

To date, the most frequently explored hydrogel materials for osteochondral tissue engineering include poly (ethylene glycol) (PEG), chitosan, hyaluronic acid, chondroitin sulfate, silk proteins, fibrin, and gelatin [12,14,26–28]. Among them, animal-derived biopolymers are biodegradable but suffer from shortcomings, such as heterogeneous compositions, inconsistent performances due to batch variations, and inherent or impurity-caused immunogenicity. Moreover, the gelation of biopolymers, taking the most widely used methacryloyl gelatin (GelMA) hydrogels as an example, often requires toxic reagents/photoinitiators. On the other hand, the degradability of synthetic polymers, such as PEG-based hydrogels, is usually unsatisfactory. More worrisome, although PEG is widely considered safe and has been extensively used for stealthy coating, mounting evidence has revealed both FBR and nonnegligible immunogenicity in PEGylated peptides, proteins, and nanocarriers [27,29–31]. Thus, the development of new biomaterial scaffolds with optimized degradability and minimized immunogenicity is a pressing and unmet clinical need.

Synthetic polypept(o)ides, or poly(amino acid)s (PAA), made by the ring-opening polymerization of amino acid *N*-carboxyanhydrides (NCA) are fascinating biomimetic polymers that can potentially harbor the advantages of both synthetic and biological polymers. The past two decades have also witnessed the rapid development of various synthetic polypept(o)ides as tissue engineering scaffolds and long-term implants [32–42]. Our previous studies have revealed that a helical polypeptide namely P(EG$_3$Glu), poly(γ-(2-(2-(2-methoxyethoxy)ethoxy) ethyl $_L$-glutamate), is a superb antifouling material when coated on various surfaces [43]. Moreover, P(EG$_3$Glu) and polysarcosine (PSar) have been used for protein conjugation, which exhibited significantly improved pharmacokinetics and reduced immunogenicity compared with analogous PEG conjugates [44–51]. Inspired by these results, we speculate that hydrogels based on the low immunogenic P(EG$_3$Glu) and PSar are promising scaffolds for osteochondral tissue engineering, which has never been attempted before.

In this study, we synthesized a novel PAA-based hydrogel with optimized degradability, good biocompatibility, and reduced immunogenicity, which together led to optimal *in vivo* performance for osteochondral repair. The hydrogel, termed as PAA-RGD, was facilely prepared by simply mixing functionalized thiol/thioester-dual functionalized P(EG$_3$Glu) and maleimide-bearing PSar under mild conditions. *In vitro*, the PAA-RGD hydrogel promoted the proliferation and chondrogenesis of MSCs. In the New Zealand White rabbit model with osteochondral defects, the MSCs-encapsulated PAA-RGD hydrogel outperformed the widely used PEG-RGD and GelMA hydrogels at both the early (week 6) and late (week 12) stages. Careful analyses of the regenerated osteochondral tissues highlighted the minimal FBR phenomenon, reduced inflammatory responses, and polarization of macrophages into immunosuppressive M2 macrophages in the PAA-RGD hydrogel-treated animals. These findings demonstrated the promising potential of PAA-RGD hydrogels for cartilage regeneration and underscored the importance of immunomodulation, which may shed light on the development of other PAA-based materials for various tissue engineering and bio-implantation applications.

2. Results and discussion

2.1. Design, synthesis, and characterization of the Polypept(o)ides

Apart from the previously mentioned biodegradability and low immunogenicity, we chose P(EG$_3$Glu) and PSar for our hydrogel preparation also because of their combined rigid-flexible molecular conformations, which may give rise to balanced mechanical and swelling performances of the hydrogels [52]. To ensure rapid gelation and induce minimal toxicity to the fragile MSC, we chose the highly efficient and reagent-free thiol-maleimide (SH-Mal) Michael addition reaction as the crosslinking chemistry. To introduce SH groups to P(EG$_3$Glu), we copolymerized γ-(2-(2-(2-methoxyethoxy) ethoxy) ethyl $_L$-glutamate NCA ($_L$-EG$_3$GluNCA) and $_L$-cysteine NCA (CysNCA), which afforded the hyperbranched polypeptide P(EG$_3$Glu-*co*-Cys) in a one-pot reaction (Fig. 1a) [53]. Apart from the facile functionalization of the thiol group for crosslinking, this concise chemistry also introduced dendritic topology with thioester as the branching site, a structural feature that was reportedly beneficial for wound healing dressings [54]. The branching thioester, thanks to its hydrolytic instability and potential thiol-thioester exchange reaction, can serve as an extra handle to accelerate the degradation of the hydrogel [55]. The product was comprehensively characterized with circular dichroism (CD) spectroscopy, size exclusion chromatography (SEC), nuclear magnetic resonance (NMR, Fig. 1b), and element analysis. Briefly, P(EG$_3$Glu-*co*-Cys) exhibited a typical α-helical secondary structure (Fig. 1c), and the molecular weight (M_n) of P(EG$_3$Glu-*co*-Cys) was measured to be ~33 kg/mol (feeding ratio of EG$_3$Glu/Cys = 5/1, Fig. 1d). P(EG$_3$Glu-*co*-Cys) contained an average of 7.5 thiol and 17.3 amine groups per chain according to the results of TNBS and Ellman's assays (see SI and Table S1 for calculation details), respectively. This result confirmed the dendritic feature of P(EG$_3$Glu-*co*-Cys), which was calculated to contain an average of 16.3 thioesters and had a degree of branching (DB) of ~0.23 (see SI and Table S1 for calculation details). The crosslinking agent, a four-armed PSar functionalized with Mal (PSar-Mal4), was next prepared as described in SI (Figs. S2–3).

2.2. Synthesis and characterization of hydrogels

To make the polypept(o)ides-based hydrogel, P(EG$_3$Glu-*co*-Cys) and PSar-Mal4 with the SH/Mal molar ratio of ~1/1 were mixed at ambient temperature in PBS, and the gelation usually finished within 1 min. To promote cell adhesion and proliferation, the integrin-binding peptide CRGD (cysteine-arginine-glycine-aspartic acid) bearing an SH group was added together with the two polypept(o)ides to generate the final hydrogel PAA-RGD (Fig. 2a). Optimization of the final concentration of RGD found that 1 mM RGD achieved the best cytoactive and chondrogenic effect [56,57]. For the control groups, we made a PEG-RGD hydrogel and a commercial GelMA hydrogel as representatives of synthetic and biological polymer hydrogels, respectively. Of note, the PEG-RGD hydrogel contained the same amount of CRGD as PAA-RGD. Due to the intrinsic cell adhesion ability of gelatin, CRGD was not introduced in GelMA.

Because cartilage needs to withstand continuous compressive stress, the anti-compression performance of the osteochondral repairing hydrogel is especially critical. Interestingly, the compression test showed that GelMA had a maximum compressive fracture strain of only ~60%, while both PAA-RGD and PEG-RGD withstood more than 90% strain (Fig. 2b and Table S2). Hydrogels for tissue engineering should have appropriate swelling ratios and excessive swelling in cartilage repair may cause buckling, slipping off, and eventually repair failure. The equilibrium swelling ratios of PAA-RGD, PEG-RGD, and GelMA were found to be ~200%, 500%, and 200%, respectively (Fig. 2c). This advantageously lower swelling ratio of PAA-RGD over PEG-RGD could be attributed to the relatively rigid chain conformation of the helical P(EG$_3$Glu-*co*-Cys) as compared to the flexible PEG. *In vitro* proteinase K-induced degradation experiments showed that the PAA-RGD hydrogel had a fast degradation rate, whereas the PEG-RGD hydrogel, not surprisingly, took the longest time for degradation (Fig. 2d). Consistently, *in vivo* degradation experiments performed by subcutaneously implanting the hydrogels into mice confirmed the trend observed *in vitro*. Briefly, the PAA-RGD hydrogels degraded completely on Day 30 after implantation, which matched the ingrowth rate of new cartilage during the repair process for a better repair effect [22]. In contrast, the complete degradation of GelMA hydrogels took approximately 60 days, and ~55% PEG-RGD hydrogel remained intact on Day 60 (Figs. S4–5).

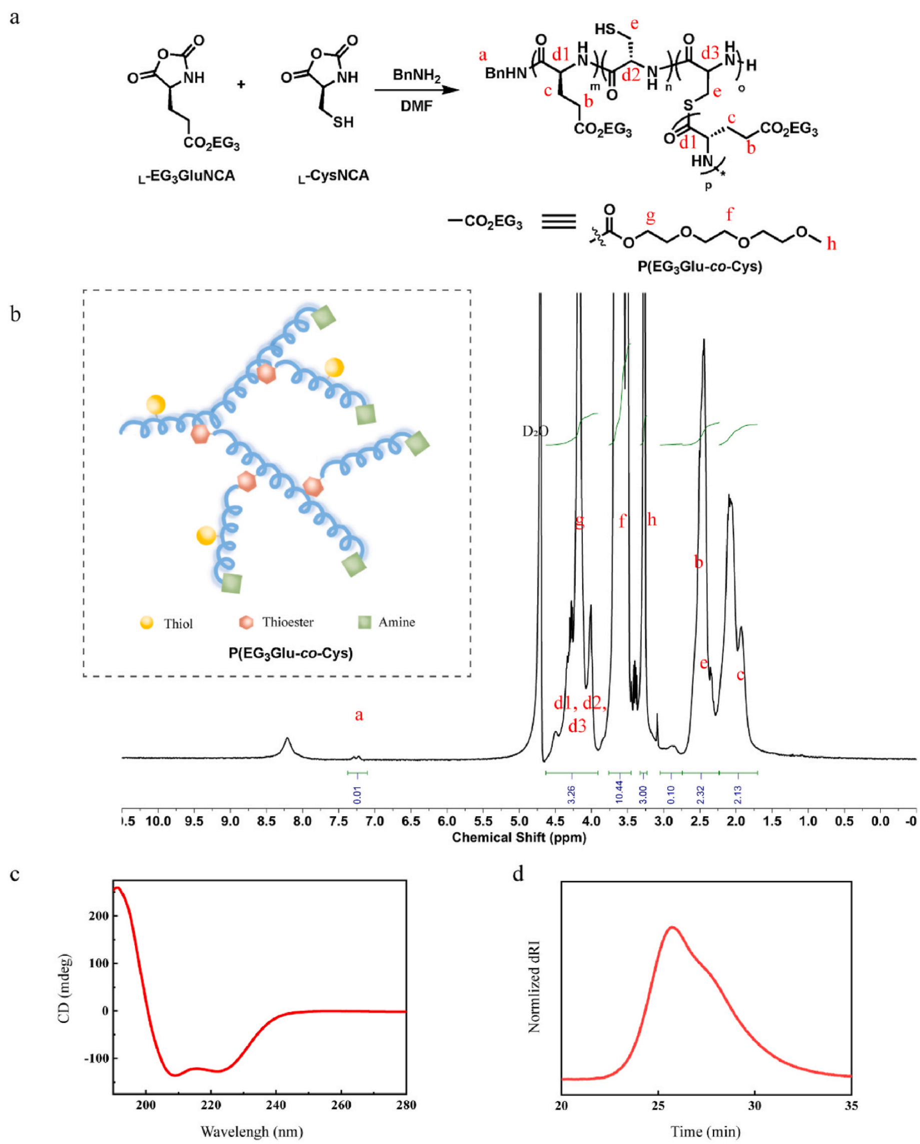

Fig. 1. Synthesis and characterization of P(EG$_3$Glu-*co*-Cys). (a) Scheme for the synthesis of P(EG$_3$Glu-*co*-Cys). (b) ^{1}H NMR spectrum (400 M, D_2O). (c) CD spectrum in H_2O (0.5 mg/mL). (d) SEC trace in DMF.

Scanning electron microscopy (SEM) found that the lyophilized PAA-RGD hydrogel showed open pores of ~200 μm in size and with irregular pore distributions, while both PEG-RGD and GelMA showed compact, regular pores of ~50 μm (Fig. 2e). The greater pore size and porous structure of the PAA-RGD hydrogel are reportedly beneficial for cartilage differentiation, cell migration, and nutrient diffusion [58,59].

2.3. In vitro stem cell proliferation and chondrogenic differentiation

To test and compare the biocompatibility of the three hydrogels, peripheral blood-derived MSCs (PB-MSCs) were seeded into the hydrogels and cultured *in vitro* [60,61]. The cell viability and proliferation of PB-MSC were measured on Day 3, 7, and 14. Both live/dead cell staining (Figs. 3a and S6a) and cell counting kit-8 (CCK-8, Figs. 3b and S6b) assays revealed that PB-MSCs were mostly survived and proliferated well in PAA-RGD and GelMA hydrogels ($P > 0.05$), whereas the PEG-RGD group showed relatively less proliferation than the other two groups ($P < 0.01$).

The chondrogenic differentiation of PBMSCs in the hydrogels was then investigated by immunofluorescence staining of the type II collagen (COL-II) expression (Fig. 3c and d). The mean fluorescence intensity of COL- II was significantly increased in the PAA-RGD group as compared to those of the PEG-PAA ($P < 0.01$) and GelMA ($P < 0.001$) groups. Quantitative reverse transcription polymerase chain reaction (qRT-PCR) also confirmed the upregulation of the chondrogenic-related genes, such as COL-II and ACAN, in the PAA-RGD group compared with PEG-RGD and GelMA groups ($P < 0.001$, Fig. 3e).

2.4. The osteochondral therapeutic efficacy in vivo

To explore the *in vivo* osteochondral regeneration, we established a rabbit osteochondral defect model (Figs. 4a and S7) with the defect sizes of ~3 × 5 mm (depth × diameter), which was 2 mm greater than the threshold diameter of spontaneous osteochondral healing [62]. PB-MSCs, isolated and cultured *in vitro*, were transplanted with PAA-RGD, PEG-RGD, or GelMA hydrogels to repair osteochondral defects (Fig. 4a). In the blank group, the osteochondral defects were seen to be filled with fibrous tissues and exhibited a severely disrupted surface at both Week 6 and 12 (Fig. 4b). PAA-RGD group exhibited optimal osteochondral repair as early as Week 6, with the defects being completely replaced with characteristic cartilage-like tissues in week 12. The repair results of the PAA-RGD hydrogel were superior to those of

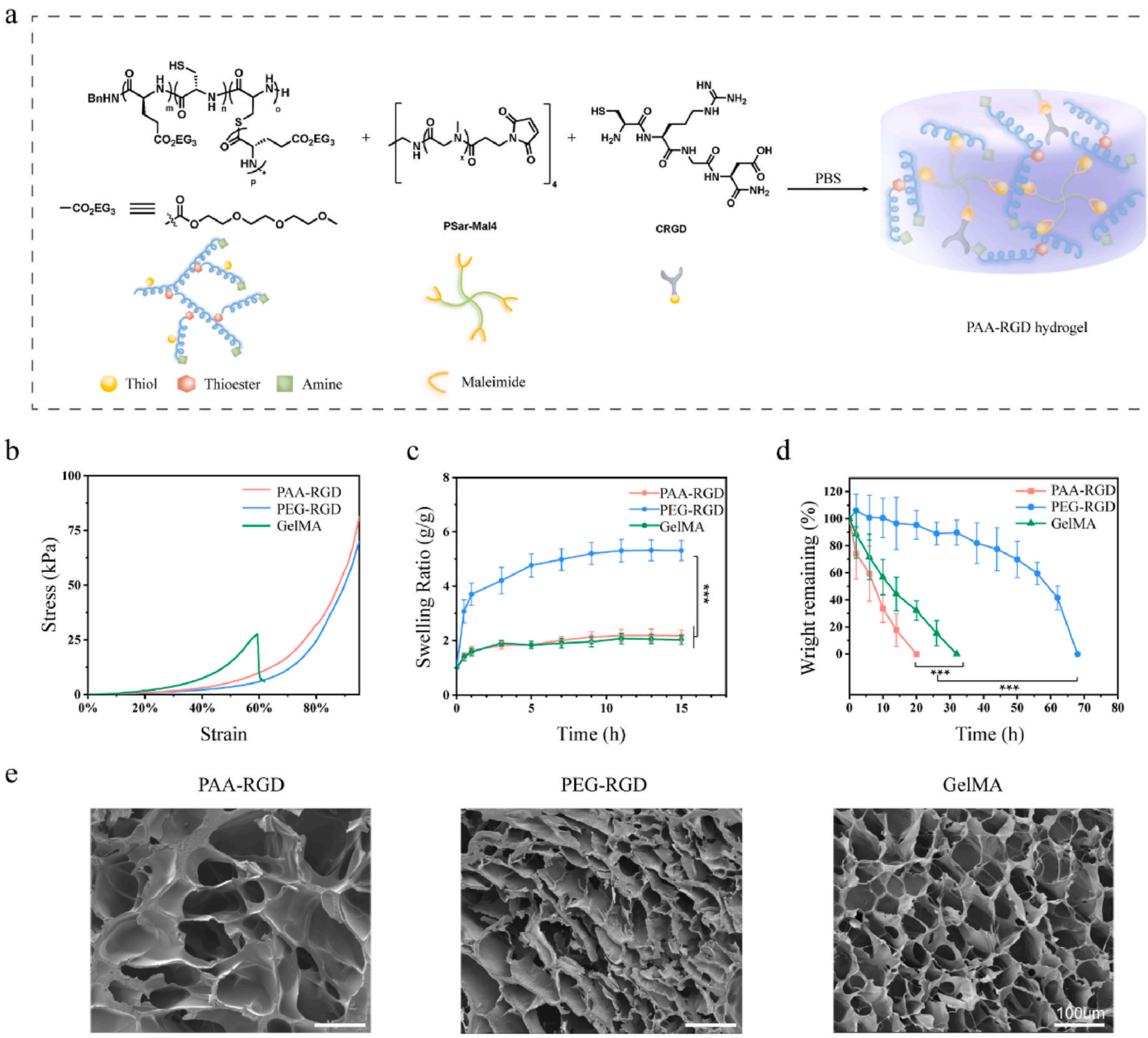

Fig. 2. Preparation and characterization of PAA-RGD, PEG-RGD, and GelMA hydrogels. (a) Cartoon illustration of the PAA-RGD hydrogel formation. (b) Strain-stress curves of the hydrogels in the compression study. (c) Swelling curves of the hydrogels ($P < 0.001$). (d) Protease K-induced degradation rate of PAA-RGD, PEG-RGD, or GelMA hydrogels *in vitro* ($P < 0.001$). (e) Representative SEM images of the hydrogels. Scale bars, 100 μm. The polymer content was fixed at 10 wt% for all of the hydrogels. Statistical significance was calculated using one-way ANOVA with Tukey's post-hoc test. ***$P < 0.001$.

both the PEG-RGD and GelMA hydrogels, particularly in Week 6, according to macroscopic observation and the scoring system of the International Cartilage Repair Society (ICRS) (Fig. 4c). In line with Figs. S4–5, the PAA-RGD hydrogel was found to be degraded completely within 6 weeks, a phenomenon that we believed to be beneficial for osteochondral regeneration. The PEG-RGD hydrogels were still observable even at week 12 (Fig. 4b), which hindered the proper tissue regeneration. GelMA, despite its popularity in the literature, showed a poor repair effect compared to PAA-RGD, particularly at the early stage (week 6).

The magnetic resonance imaging (MRI) results echoed the above findings (Fig. 4d). In the PAA-RGD group, the cartilage showed smoother surfaces and less subchondral bone edema, whereas both the PEG-RGD and GelMA groups showed cartilage surface interruption and significantly increased subchondral bone edema signals. Moreover, the subchondral bone repair in the PAA-RGD group was also superior to that in all other control groups, as analyzed by micro-computed tomography (micro-CT, Fig. 4e). In addition, evaluation of the trabecular bone volume fraction (BV/TV), trabecular number (Tb. N), and trabecular separation (Tb. Sp) also revealed prominently improved subchondral bone formation for the PAA-RGD hydrogel group (Fig. S8). Again, the PAA-RGD hydrogel showed its superior ability to heal cartilage and subchondral bone from as early as Week 6 in all the above evaluations, which was not achieved for either GelMA or PEG-RGD.

Next, SEM was performed to observe the microstructure of the repaired cartilage surfaces. The PAA-RGD group exhibited smooth, crackless, and homogeneous surfaces that were similar to the microstructure of normal cartilages at Week 12 after surgery (Fig. 5a). In contrast, both the PEG-RGD and GelMA groups had rugged cartilage surfaces and/or obvious cracks. Staining of Hematoxylin-eosin (H&E, histomorphology of osteochondral tissue), toluidine blue (TB, cartilage glycosaminoglycan), safranin O-fast green (SO, cartilage glycosaminoglycan & FG, bone tissue and collagen fibers), and immunohistochemistry of COL-II regeneration further validated the superior repairing results of PAA-RGD in both weeks 6 and 12 (Figs. 5b and S9). Specifically, it was found that the PAA-RGD hydrogel-treated osteochondral tissues were fully repaired with a smooth surface, characteristic chondrocyte arrangement, and homogenous matrix deposition. Although the GelMA group showed a relatively normal osteochondral morphology in week 12, the morphology of cartilage and bone formation at Week 6 was delayed due to slow degradation of the hydrogel as compared to PAA-RGD. Moreover, the cartilage-bone interfaces of GelMA were less regular than those of the PAA-RGD group in both weeks 6 and 12. The PEG-RGD hydrogel-treated cartilage samples were observed to be

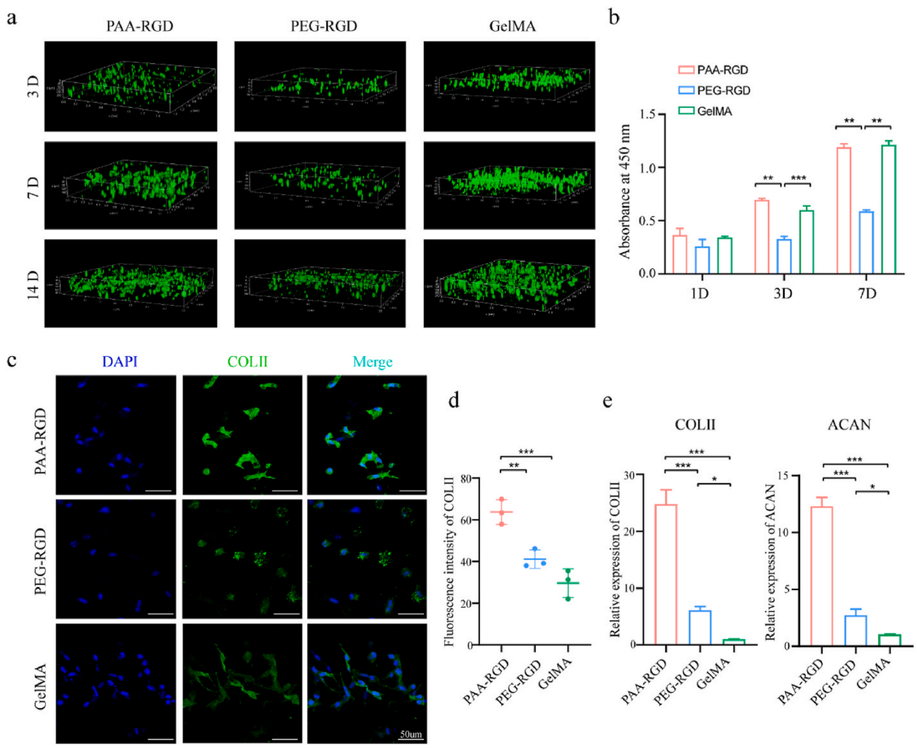

Fig. 3. The proliferation and chondrogenic differentiation of PB-MSCs in PAA-RGD, PEG-RGD, and GelMA hydrogels. (a) Cell proliferation and Live/Dead staining in 3D plots after 3, 7, and 14 days of culture live cells: green; dead cells: red). (b) Cell proliferation determined by CCK8 assay. (c–d) Immunofluorescence staining (c) and quantification (d) of COL-II expression in PB-MSCs-encapsulating hydrogels on Day 14 following chondrogenic induction; scale bar = 50 μm; (Relative fluorescence intensity was quantified using *Image J* software). (e) The relative mRNA expression of chondrogenic genes (COL-II, and ACAN) on Day 7 after chondrogenic induction. Data are presented as the mean ± S.D. ($n \geq 3$). Statistical significance was calculated using one-way ANOVA with Tukey's post-hoc test. *$P < 0.05$, **$P < 0.01$, ***$P < 0.001$.

encapsulated with a layer of dense connective or fibrous tissues.

2.5. Cartilage repair validation at genetic and molecular levels

To further validate the cartilage repair, the regenerated cartilage tissues were harvested at Week 12 after surgery to interrogate the mRNA expression. Principal component analysis (PCA) revealed a similar mRNA transcriptome pattern of the PAA-RGD hydrogel-repaired newborn cartilage and native cartilage, whereas the PEG-RGD and GelMA groups showed mRNA expression characteristics that were quite distinct from the native ones (Fig. 6a). It should be pointed out that within the GelMA group, the mRNA expression exhibited vast variations between individual animals, which might be attributable to the complexity and heterogeneity of GelMA in both primary sequence, molecular weight, and dispersity.

Interestingly, gene ontology (GO) enrichment analysis suggested that the differentially expressed genes in PEG-RGD and GelMA-treated cartilage tissue samples were mostly involved in the immune response, inflammatory response, and lipopolysaccharide-mediated signaling pathways ($P < 0.001$), which all have been reported to participate in the progression of inflammation (Fig. 6b and c). In consistent with the GO enrichment results, the Kyoto Encyclopedia of Genes and Genomes (KEGG) pathway enrichment analysis also indicated that the chemokine signaling pathway, Toll-like receptor signaling pathway, graft-versus-host disease, and allograft rejections ($P < 0.01$) were downregulated in the PAA-RGD group as compared to those of the PEG-RGD and GelMA groups (Fig. 6d and e). Moreover, the hierarchical clustering analysis also implied upregulation of graft-versus-host disease pathways in the PEG-RGD and GelMA groups (Fig. 6f). Thus, it appeared that the PAA-RGD hydrogel was less immunogenic and evoked fewer inflammatory responses than the PEG-RGD and GelMA hydrogels, which likely contributed to the superior osteochondral regeneration.

2.6. The immune response and the FBR of hydrogels in mice

Inspired by the results of the rabbit osteochondral repair model, we further evaluated the immune response and the FBR in C57/BL6 mice subcutaneously implanted with PAA-RGD, PEG-RGD, or GelMA hydrogels for 14 days (Fig. 7a). H&E staining of the tissues around the hydrogels showed the fewest cells for the PAA-RGD group and the most cells around the GelMA group (Fig. 7b). Masson's trichrome (M&T) staining showed only a small amount of sparse collagen around the PAA-RGD hydrogel with no obvious signs of FBR, whereas a dense fibrous sac was visible around both GelMA and PEG-RGD hydrogels, indicating characteristic FBR (Fig. 7b).

The surface of biomaterials can regulate the macrophage phenotype to modulate host responses to the implants [63]. To further explore the immunomodulatory role of different hydrogels, immunohistochemical observations were performed to assess the phenotype of macrophages infiltrated into tissues near the hydrogels (Figs. 7c and S10). Macrophages that infiltrated around the PAA-RGD hydrogel were mostly the immunosuppressive $CD206^+$ M2 phenotype, whereas the PEG-RGD hydrogel had a significantly higher ratio of immune-stimulating $CD86^+$ M1 phenotype macrophages. The implanted GelMA hydrogel did not significantly alter the macrophage polarization *in vivo*, which was comparable to previous reports [64]. The macrophage polarization results were further verified using qRT-PCR, in which the PAA-RGD group showed significantly upregulated expression of M2 phenotype genes, such as IL-10 and Arg (Fig. 7d), and downregulated expression of M1 phenotype genes, such as IL-1 and INOS (Fig. 7e). Given that previous studies have shown that the anti-inflammatory M2 macrophages are conducive to tissue remodeling and repair [65], we considered this to be an important factor responsible for the superior osteochondral repair outcomes of the PAA-RGD hydrogel.

3. Conclusion

In summary, we synthesized a polypept(o)ide-based PAA-RGD hydrogel using a novel thiol/thioester dual-functionalized hyperbranched polypeptide P(EG_3Glu-*co*-Cys) and maleimide-functionalized PSar under biologically benign conditions. The hydrogel showed a porous morphology, suitable biodegradation profile, and low swelling ratio, which are desirable for osteochondral repair. *In vitro*, the PAA-RGD hydrogel exhibited excellent biocompatibility and promoted the

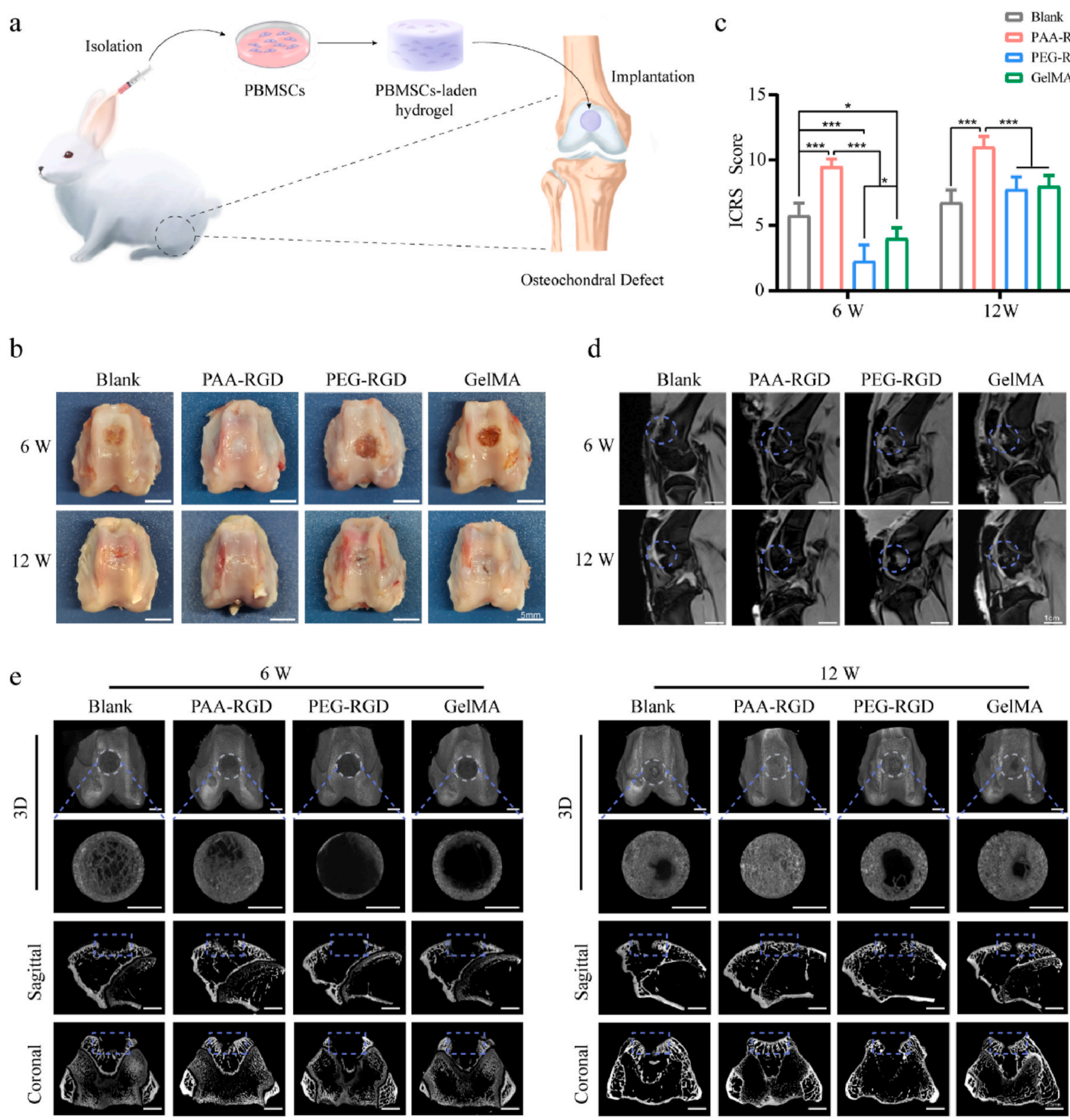

Fig. 4. The repair efficacy of osteochondral defects by PBMSCs-encapsulated hydrogels *in vivo*. (a) The operation flowchart of PBMSCs isolation, encapsulation, and hydrogel implantation into osteochondral defects. (b) The macroscopic appearance of the repaired joint; scale bar = 5 mm. (c) ICRS macroscopic assessment scores in osteochondral repair. Data are presented as the mean ± S.D. (n = 4). Statistical significance was calculated using two-way ANOVA with Tukey's post-hoc test. *$P < 0.05$, ***$P < 0.001$. (d) The MRI scan of the repaired knee joints; scale bars = 1 cm. (e) Representative micro-CT images of subchondral bone repair at 6 and 12 weeks after treatment; scale bar = 2.5 mm.

chondrogenesis of PBMSCs. Comprehensively evaluated using various technologies, the PBMSCs-encapsulated PAA-RGD hydrogel displayed unambiguously superior osteochondral repair results over PEG-RGD and GelMA hydrogels in New Zealand white rabbits, especially at early stages (e.g. week 6). Further bioinformatics analysis showed that the new cartilage treated with the PAA-RGD hydrogel significantly reduced the intra-articular immune responses compared with PEG-RGD and GelMA hydrogels. The immunomodulatory performances of the PAA-RGD hydrogel were further validated in C57/BL6 mice subcutaneously implanted with hydrogels, which indicated that the PAA-RGD hydrogel induced the least FBR response and the most polarization of macrophages into the immunosuppressive M2 subtypes. These findings demonstrated the promising potential of PAA-RGD hydrogel for osteochondral regeneration and underscored the importance of immunomodulation, which may inspire the development of other PAA-based materials for various tissue engineering and bio-implantation applications.

4. Methods

4.1. Preparation of the PAA-RGD hydrogel

The general procedure for polypeptides was modified from reported methods [53] and details were described in the SI. Stock solutions of P(EG$_3$Glu-*co*-Cys) (solution A, 100 mg/mL), PSar-Mal4 (solution B, 150 mg/mL) and CRGD (solution C, 20 mg/mL) were prepared in advance using PBS (pH = 7.4). The stock solutions need to pass a 0.22 μm diameter sterilizing filter membrane. In a typical experiment, 55 μL of A, 30 μL of B (thiol: maleimide = 1:1), and 15 μL of PBS were mixed together by pipetting to make a 10 wt% hydrogel of 100 μL. To make a CRGD-containing gel, 52 μL of A, 32 μL of B, 2 μL of C (total thiol: maleimide = 1:1) and 14 μL of PBS were mixed together by pipetting to

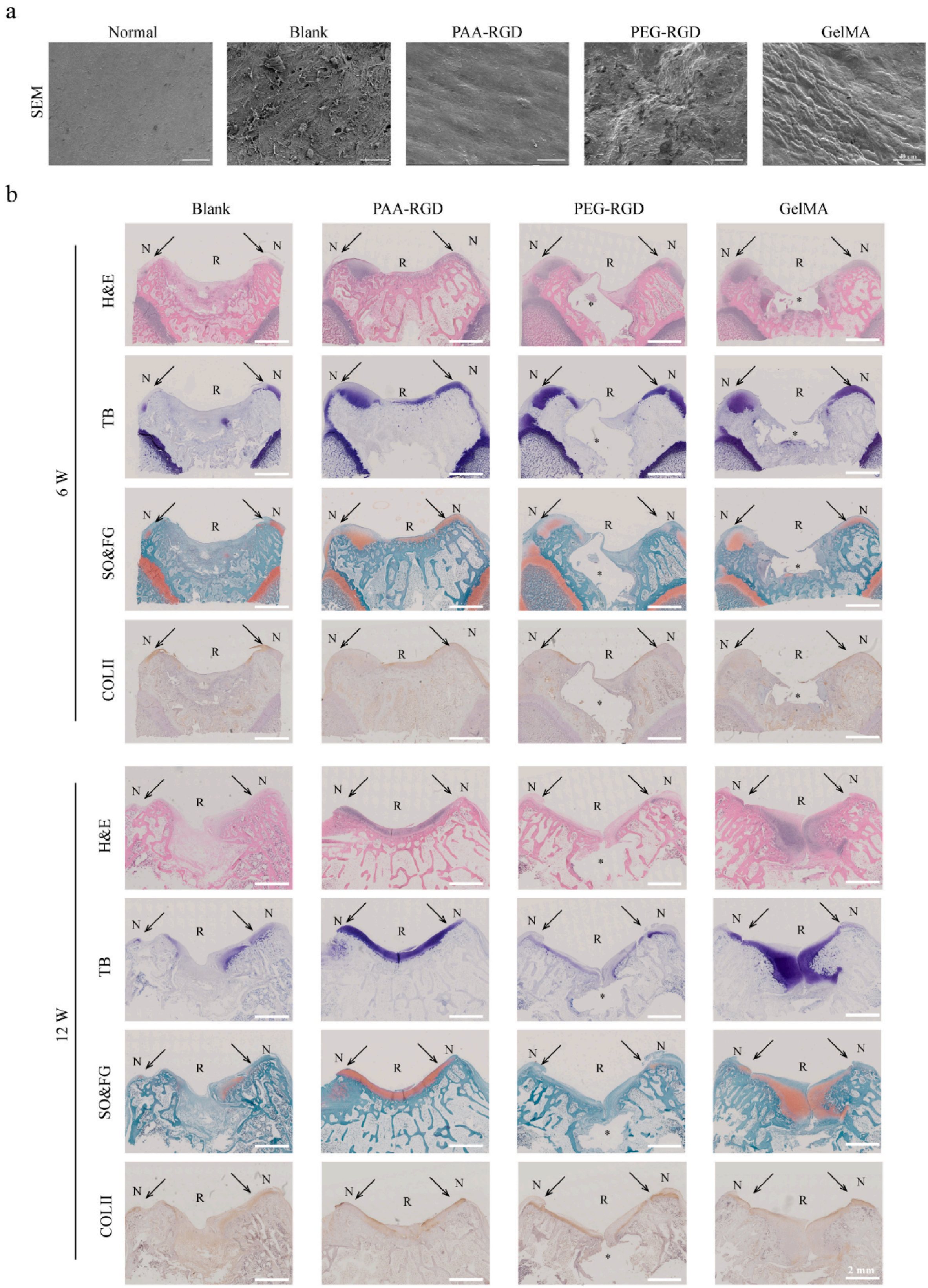

Fig. 5. Morphology, histology, and immunohistochemistry of the repaired cartilages. (a) SEM images of representative repaired cartilage surfaces 12 weeks after treatments. scale bar = 40 μm. (b) H&E, Toluidine Blue (purple), Safranin O-Fast Green (orange & green), and immunohistochemistry staining showing the COL-II regeneration (brown); scale bar = 2 mm, * = the nondegraded part of the hydrogel, N = normal cartilage, R = repaired tissues, the arrows indicated the interfaces of the normal cartilages and repaired tissues.

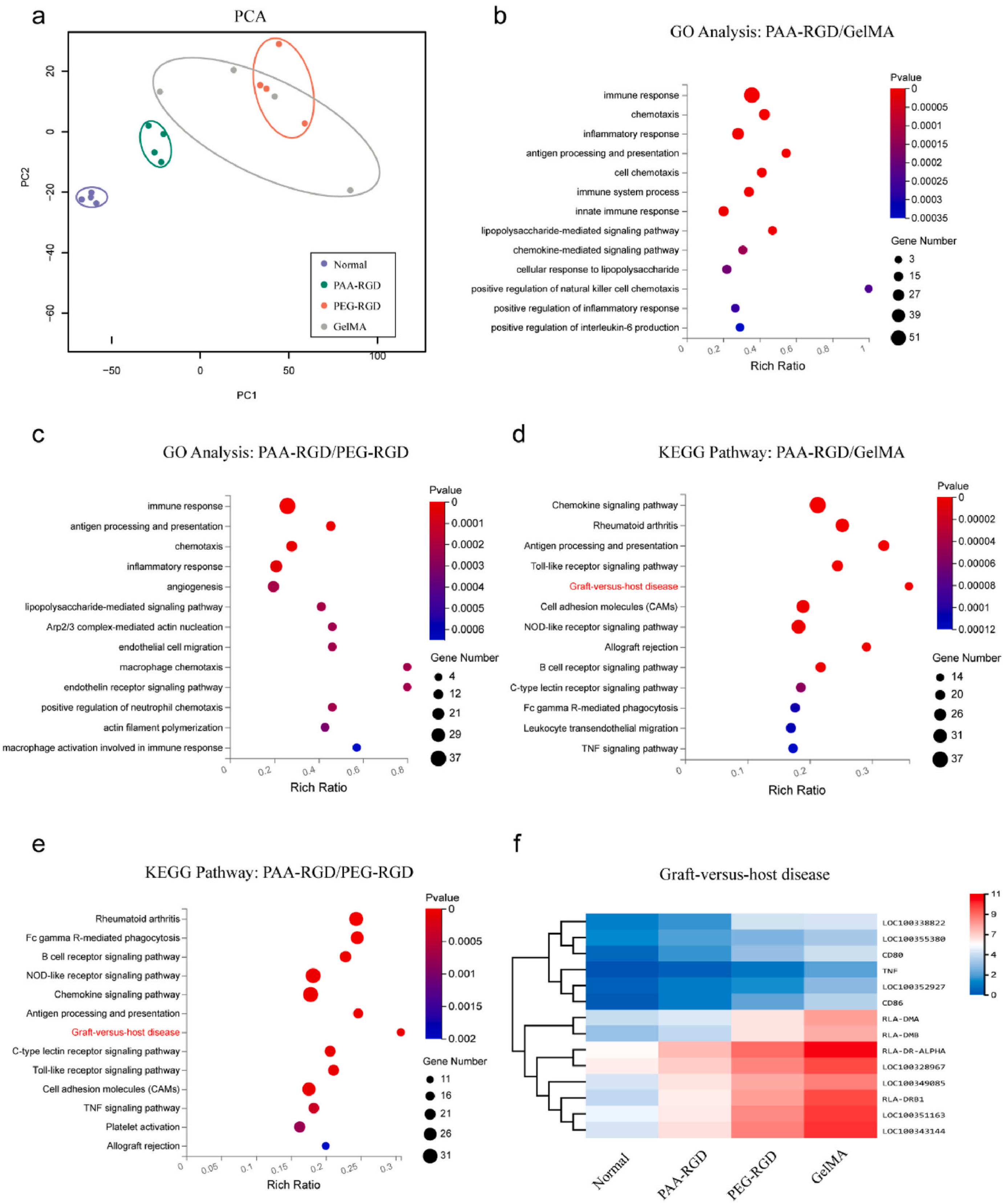

Fig. 6. RNA sequencing of the repaired articular cartilages at week 12. (a) Principal component analysis (PCA) of the cartilage transcriptome from the normal, PAA-RGD, PEG-RGD, and GelMA groups. (b–c) Gene ontology (GO) pathway analysis of genes downregulated in the PAA-RGD group as relative to the GelMA (b) and PEG-RGD (c) groups. (d–e) KEGG pathway analysis of genes downregulated in the PAA-RGD group as relative to the GelMA (d) and PEG-RGD (e) groups. (f) Hierarchical clustering analysis using differentially expressed genes implied downregulated graft-versus-host disease pathways for the PAA-RGD group.

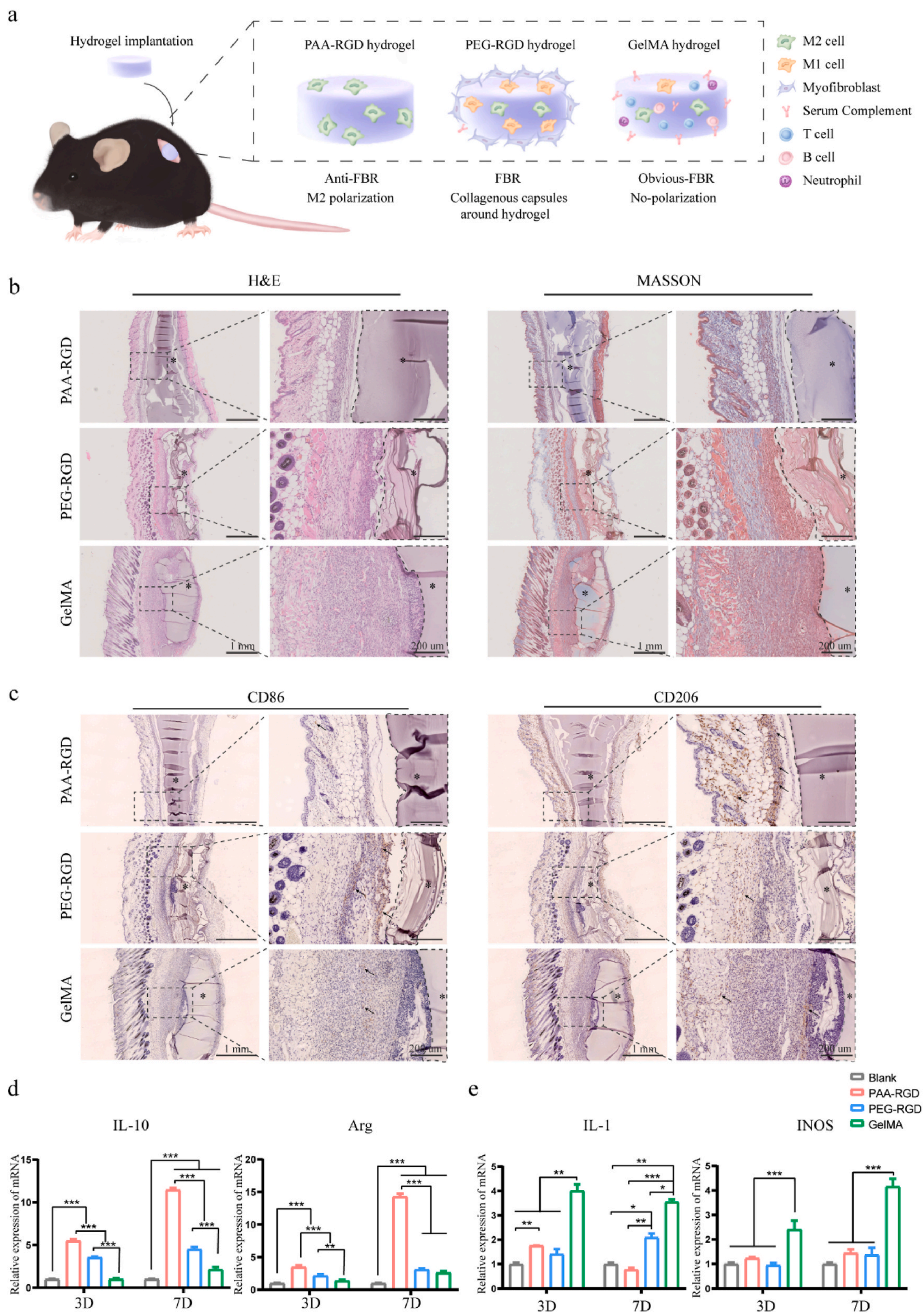

Fig. 7. FBR and macrophage polarization of various hydrogels implanted in mice and RAW264.7 cells. (a) Cartoon illustration of FBR and macrophages polarization in C57/BL6 mice induced by the subcutaneously implanted hydrogels. (b) HE and MASSON staining were used to evaluate the inflammatory response and collagen encapsulation density after 14 days after implantation. Scale bars, 1 mm, 200 μm; * = hydrogels. (c) Immunohistochemical staining to assess the phenotype of macrophages infiltrated into hydrogels-tissues interfaces on Day14 after implantation. Positive staining is observed as a brown color (Representative positive cells indicated by arrows), while all nucleus stained with hematoxylin show blue color. Scale bars, 1 mm, 200 μm; * = hydrogels. (d–e) The mRNA levels of the representative M2 macrophages biomarkers IL-10 and Arg (d) and the characteristic M1 macrophages biomarkers IL-1 and iNOS (e). RAW 264.7 cells were treated with various hydrogels for 3 and 7 days before harvesting and analyzed by qRT-PCR. Data are presented as the mean ± S.D. (n ≥ 3). Statistical significance was calculated using two-way ANOVA with Tukey's post-hoc test. *$P < 0.05$, **$P < 0.01$, ***$P < 0.001$.

make a 10 wt% hydrogel of 100 μL. The gelation occurred immediately and usually finished within 1 min.

4.2. Preparation of 4A-polyethylene glycol (PEG) hydrogel

Stock solutions of PEG-SH4 (solution A, 100 mg/mL), PEG-Mal4 (solution B, 100 mg/mL) and CRGD (solution C, 20 mg/mL) were prepared in advance using PBS (pH = 7.4). The stock solutions need to pass a 0.22 μm diameter sterilizing filter membrane. In a typical experiment, 50 μL of A, 50 μL of B (thiol: maleimide = 1:1) were mixed together by pipetting to make a 10 wt% hydrogel of 100 μL. To make a CRGD-containing gel, 48 μL of A, 50 μL of B, 2 μL of C (total thiol: maleimide = 1:1) were mixed together by pipetting to make a 10 wt% hydrogel of 100 μL. The gelation occurred immediately and usually finished within 1 min.

4.3. Preparation of methyl acrylylated gelatin (GelMA) hydrogel

A working solution of LAP (0.5 wt%) was prepared in advance using PBS (pH = 7.4). The stock solutions need to pass a 0.22 μm diameter sterilizing filter membrane. In a typical experiment, 10 mg of GelMA sponge was dissolved in 90 μL of LAP working solution. After complete dissolution, the mixture was exposed to blue light radiation (365 nm) at 37 °C. The gelation occurred in seconds and finished within 1 min.

4.4. Swelling experiment of the hydrogels

Before the study, the weight (W_d) of each wet hydrogel sample (10 wt%, 50 μL) was recorded. To the hydrogels, we then added 5 mL PBS and incubated at 37 °C for a certain period of time (0.5, 1, 3, 5, 7, 9, 11, 13, 15 h, respectively). The weight of the swelled hydrogels was recorded (W_s). The swelling ratio (SR) was calculated by using the following equation:

$$SR = (W_s - W_d)/W_d$$

4.5. In vitro degradation of the hydrogels

Before the study, each wet hydrogel sample (10 wt%, 50 μL) was lyophilized and the weight (W_0) was recorded. Protease K solution (0.05 mg/mL) was prepared using PBS (pH = 7.4). Then, the dry hydrogels were incubated in protease K solution at 37 °C for a certain period of time (2, 6, 10, 14, 20, 26, 32, 38, 44, 50, 56, 62, and 68 h), while the medium was exchanged for every 4 h. After each period, the hydrogel was lyophilized, and the weight was recorded (W_d). The percentage of mass remaining (MR) was calculated by using the following equation:

$$MR(\%) = \left(\frac{W_d}{W_0}\right) \times 100\%$$

4.6. In vivo osteochondral repair in New Zealand white rabbits

Before surgery, the adult New Zealand rabbits weighing 3.0–3.5 kg were shaved, and routinely disinfected, and the knee joint was exposed through a medial parapatellar approach and lateral patellar dislocation after the anesthesia. To create the osteochondral defect model, a full-thickness defect of 5 mm in diameter and 3 mm in depth was created using a corneal trephine on the articular cartilage of the trochlear groove of the distal femur. The PBMSCs-loaded hydrogels (50,00 cells in 50 μL hydrogels) were then embedded into the defect area, with the blank control undergoing no intervention. The subcutaneous tissues and skin were sutured layer by layer. Next, all of the rabbits received antibiotic prophylaxis and analgesia. On recovery, the rabbits were allowed free spontaneous activity in the cage. Rabbits of each group were euthanized at 6 and 12 weeks. Knee joint samples were collected for subsequent experiments.

4.7. FBR evaluation in hydrogel-implanted C57/BL6 mice

After the anesthesia, hydrogels (10 wt%, 50 μL) were implanted subcutaneously into the dorsal flank of female C57/BL6 mice (4–6 weeks). On recovery, mice were allowed free spontaneous activity in the cage. Mice in each group were euthanized on Day 14. Then, the hydrogel and skin tissues surrounding the hydrogel were surgically separated and observed.

4.8. Statistical analysis

Each experiment was repeated at least in triplicate. Statistical analysis among groups was conducted using one-way ANOVA with Tukey's post-hoc test or two-way ANOVA with Tukey's post-hoc test. All data analyses were calculated using SPSS 22.0 software. The value of $P < 0.05$ was considered statistically significant.

Ethics approval and consent to participate

This study didn't involve human participants, data, and biological materials.

All animal experiments were approved by the Ethical Committee of Laboratory Animals of Peking University Third Medical School (No. A2019029) and all the procedures were conducted following the guidelines of the Care and Use of Laboratory Animals.

CRediT authorship contribution statement

Meng Yang: Investigation, Data curation, Visualization, Methodology, Formal analysis, Writing – original draft. **Zheng-Chu Zhang:** Conceptualization, Investigation, Data curation, Methodology, Writing – original draft. **Fu-Zhen Yuan:** Investigation, Data curation, Methodology, Funding acquisition, Writing – review & editing. **Rong-Hui Deng:** Formal analysis, Writing – review & editing. **Xin Yan:** Writing – review & editing. **Feng-Biao Mao:** Writing – review & editing. **You-Rong Chen:** Methodology, Conceptualization, Funding acquisition, Writing – review & editing. **Hua Lu:** Conceptualization, Funding acquisition, Supervision, Writing – review & editing. **Jia-Kuo Yu:** Conceptualization, Funding acquisition, Visualization, Supervision, Project administration, Writing – review & editing.

Declaration of competing interest

The authors declare that they have no known competing financial interests or personal relationships that could have appeared to influence the work reported in this paper.

Acknowledgements

This work was supported by the Beijing Natural Science Foundation (L192066), the National Natural Science Foundation of China (22125101, 51773004, 51920105006, 82102565, 52003008) and the Construction of a Basic Public Service Platform for Industrial Technology in the Field of Advanced Medical Equipment (0714-EMTC-02-00897). All authors reviewed and commented on the manuscript.

Appendix A. Supplementary data

Supplementary data to this article can be found online at https://doi.org/10.1016/j.bioactmat.2022.05.008.

References

[1] W. Wei, H. Dai, Articular cartilage and osteochondral tissue engineering techniques: recent advances and challenges, Bioact. Mater. 6 (2021) 4830–4855, https://doi.org/10.1016/j.bioactmat.2021.05.011.

[2] K. Zha, X. Li, Z. Yang, G. Tian, Z. Sun, X. Sui, Y. Dai, S. Liu, Q. Guo, Heterogeneity of mesenchymal stem cells in cartilage regeneration: from characterization to application, npj Regener. Med. 6 (2021) 14, https://doi.org/10.1038/s41536-021-00122-6.
[3] Y. Xiang, V. Bunpetch, W. Zhou, H. Ouyang, Optimization strategies for ACI: a step-chronicle review, J. Orthop Translat. 17 (2019) 3–14, https://doi.org/10.1016/j.jot.2018.12.005.
[4] K.N. Kunze, J.S. Manzi, J. Wright-Chisem, P. Ramkumar, B.U. Nwachukwu, R. R. Williams, Risk factors for failure after osteochondral allograft transplantation of the knee: a systematic review and exploratory meta-analysis, Am. J. Sports Med. (2022), https://doi.org/10.1177/03635465211063901, 3635465211063901.
[5] H. Cao, X. Wang, M. Chen, Y. Liu, X. Cui, J. Liang, Q. Wang, Y. Fan, X. Zhang, Childhood cartilage ECM enhances the chondrogenesis of endogenous cells and subchondral bone repair of the unidirectional collagen-dECM scaffolds in combination with microfracture, ACS Appl. Mater. Interfaces 13 (2021) 57043–57057, https://doi.org/10.1021/acsami.1c19447.
[6] K.E. Martin, A.J. García, Macrophage phenotypes in tissue repair and the foreign body response: implications for biomaterial-based regenerative medicine strategies, Acta Biomater. 133 (2021) 4–16, https://doi.org/10.1016/j.actbio.2021.03.038.
[7] C. Ai, Y. Lee, X.H. Tan, S. Tan, J. Hui, J.C. Goh, Osteochondral tissue engineering: perspectives for clinical application and preclinical development, J. Orthop Translat. 30 (2021) 93–102, https://doi.org/10.1016/j.jot.2021.07.008.
[8] A. Khademhosseini, R. Langer, A decade of progress in tissue engineering, Nat. Protoc. 11 (2016) 1775–1781, https://doi.org/10.1038/nprot.2016.123.
[9] A.C. Daly, L. Riley, T. Segura, J.A. Burdick, Hydrogel microparticles for biomedical applications, Nat. Rev. Mater. 5 (2020) 20–43, https://doi.org/10.1038/s41578-019-0148-6.
[10] W. He, M. Reaume, M. Hennenfent, B.P. Lee, R. Rajachar, Biomimetic hydrogels with spatial- and temporal-controlled chemical cues for tissue engineering, Biomater. Sci. 8 (2020) 3248–3269, https://doi.org/10.1039/d0bm00263a.
[11] A.S. Caldwell, B.A. Aguado, K.S. Anseth, Designing microgels for cell culture and controlled assembly of tissue microenvironments, Adv. Funct. Mater. 30 (2020), https://doi.org/10.1002/adfm.201907670.
[12] C. Schuurmans, M. Mihajlovic, C. Hiemstra, K. Ito, W.E. Hennink, T. Vermonden, Hyaluronic acid and chondroitin sulfate (meth)acrylate-based hydrogels for tissue engineering: synthesis, characteristics and pre-clinical evaluation, Biomaterials 268 (2021), 120602, https://doi.org/10.1016/j.biomaterials.2020.120602.
[13] A. Kirillova, T.R. Yeazel, D. Asheghali, S.R. Petersen, S. Dort, K. Gall, M.L. Becker, Fabrication of biomedical scaffolds using biodegradable polymers, Chem. Rev. 121 (2021) 11238–11304, https://doi.org/10.1021/acs.chemrev.0c01200.
[14] J. Shi, L. Yu, J. Ding, PEG-based thermosensitive and biodegradable hydrogels, Acta Biomater. 128 (2021) 42–59, https://doi.org/10.1016/j.actbio.2021.04.009.
[15] X. Du, Y. Liu, H. Yan, M. Rafique, S. Li, X. Shan, L. Wu, M. Qiao, D. Kong, L. Wang, Anti-infective and pro-coagulant chitosan-based hydrogel tissue adhesive for sutureless wound closure, Biomacromolecules 21 (2020) 1243–1253, https://doi.org/10.1021/acs.biomac.9b01707.
[16] F. Gao, Z. Xu, Q. Liang, H. Li, L. Peng, M. Wu, X. Zhao, X. Cui, C. Ruan, W. Liu, Osteochondral regeneration with 3D-printed biodegradable high-strength supramolecular polymer reinforced-gelatin hydrogel scaffolds, Adv. Sci. 6 (2019), 1900867, https://doi.org/10.1002/advs.201900867.
[17] Q. Li, L. Ma, C. Gao, Biomaterials for in situ tissue regeneration: development and perspectives, J. Mater. Chem. B 3 (2015) 8921–8938, https://doi.org/10.1039/c5tb01863c.
[18] F. Sun, Y. Bu, Y. Chen, F. Yang, J. Yu, D. Wu, An injectable and instant self-healing medical adhesive for wound sealing, ACS Appl. Mater. Interfaces 12 (2020) 9132–9140, https://doi.org/10.1021/acsami.0c01022.
[19] Y. He, Q. Li, C. Ma, D. Xie, L. Li, Y. Zhao, D. Shan, S.K. Chomos, C. Dong, J. W. Tierney, L. Sun, D. Lu, L. Gui, J. Yang, Development of osteopromotive poly (octamethylene citrate glycerophosphate) for enhanced bone regeneration, Acta Biomater. 93 (2019) 180–191, https://doi.org/10.1016/j.actbio.2019.03.050.
[20] J.N. Fu, X. Wang, M. Yang, Y.R. Chen, J.Y. Zhang, R.H. Deng, Z.N. Zhang, J.K. Yu, F.Z. Yuan, Scaffold-based tissue engineering strategies for osteochondral repair, Front. Bioeng. Biotechnol. 9 (2021), 812383, https://doi.org/10.3389/fbioe.2021.812383.
[21] K. Zhou, P. Yu, X. Shi, T. Ling, W. Zeng, A. Chen, W. Yang, Z. Zhou, Hierarchically porous hydroxyapatite hybrid scaffold incorporated with reduced graphene oxide for rapid bone ingrowth and repair, ACS Nano 13 (2019) 9595–9606, https://doi.org/10.1021/acsnano.9b04723.
[22] H. Seyednejad, W. Ji, W. Schuurman, W.J. Dhert, J. Malda, F. Yang, J.A. Jansen, C. van Nostrum, T. Vermonden, W.E. Hennink, An electrospun degradable scaffold based on a novel hydrophilic polyester for tissue-engineering applications, Macromol. Biosci. 11 (2011) 1684–1692, https://doi.org/10.1002/mabi.201100229.
[23] Z. Yang, H. Li, Y. Tian, L. Fu, C. Gao, T. Zhao, F. Cao, Z. Liao, Z. Yuan, S. Liu, Q. Guo, Biofunctionalized structure and ingredient mimicking scaffolds achieving recruitment and chondrogenesis for staged cartilage regeneration, Front. Cell Dev. Biol. 9 (2021), 655440, https://doi.org/10.3389/fcell.2021.655440.
[24] B. Zhang, Y. Su, J. Zhou, Y. Zheng, D. Zhu, Toward a better regeneration through implant-mediated immunomodulation: harnessing the immune responses, Adv. Sci. 8 (2021), e2100446, https://doi.org/10.1002/advs.202100446.
[25] N.G. Welch, D.A. Winkler, H. Thissen, Antifibrotic strategies for medical devices, Adv. Drug Deliv. Rev. 167 (2020) 109–120, https://doi.org/10.1016/j.addr.2020.06.008.
[26] P. Li, L. Fu, Z. Liao, Y. Peng, C. Ning, C. Gao, D. Zhang, X. Sui, Y. Lin, S. Liu, C. Hao, Q. Guo, Chitosan hydrogel/3D-printed poly(ε-caprolactone) hybrid scaffold containing synovial mesenchymal stem cells for cartilage regeneration based on tetrahedral framework nucleic acid recruitment, Biomaterials 278 (2021), 121131, https://doi.org/10.1016/j.biomaterials.2021.121131.
[27] H. Hong, Y.B. Seo, D.Y. Kim, J.S. Lee, Y.J. Lee, H. Lee, O. Ajiteru, M.T. Sultan, O. J. Lee, S.H. Kim, C.H. Park, Digital light processing 3D printed silk fibroin hydrogel for cartilage tissue engineering, Biomaterials 232 (2020), 119679, https://doi.org/10.1016/j.biomaterials.2019.119679.
[28] Q. Li, S. Xu, Q. Feng, Q. Dai, L. Yao, Y. Zhang, H. Gao, H. Dong, D. Chen, X. Cao, 3D printed silk-gelatin hydrogel scaffold with different porous structure and cell seeding strategy for cartilage regeneration, Bioact. Mater. 6 (2021) 3396–3410, https://doi.org/10.1016/j.bioactmat.2021.03.013.
[29] P. Zhang, F. Sun, S. Liu, S. Jiang, Anti-PEG antibodies in the clinic: current issues and beyond PEGylation, J. Contr. Release 244 (2016) 184–193, https://doi.org/10.1016/j.jconrel.2016.06.040.
[30] I. Ekladious, Y.L. Colson, M.W. Grinstaff, Polymer-drug conjugate therapeutics: advances, insights and prospects, Nat. Rev. Drug Discov. 18 (2019) 273–294, https://doi.org/10.1038/s41573-018-0005-0.
[31] K. Knop, R. Hoogenboom, D. Fischer, U.S. Schubert, Poly(ethylene glycol) in drug delivery: pros and cons as well as potential alternatives, Angew. Chem., Int. Ed. Engl. 49 (2010) 6288–6308, https://doi.org/10.1002/anie.200902672.
[32] A.P. Nowak, V. Breedveld, L. Pakstis, B. Ozbas, D.J. Pine, D. Pochan, T.J. Deming, Rapidly recovering hydrogel scaffolds from self-assembling diblock copolypeptide amphiphiles, Nature 417 (2002) 424–428, https://doi.org/10.1038/417424a.
[33] H. He, M. Sofman, A.J. Wang, C.C. Ahrens, W. Wang, L.G. Griffith, P.T. Hammond, Engineering helical modular polypeptide-based hydrogels as synthetic extracellular matrices for cell culture, Biomacromolecules 21 (2020) 566–580, https://doi.org/10.1021/acs.biomac.9b01297.
[34] L. Yin, J. Cheng, T.J. Deming, M.J. Vicent, Synthetic polypeptides for drug and gene delivery, and tissue engineering, Adv. Drug Deliv. Rev. 178 (2021), 113995, https://doi.org/10.1016/j.addr.2021.113995.
[35] H. Liu, Y. Cheng, J. Chen, F. Chang, J. Wang, J. Ding, X. Chen, Component effect of stem cell-loaded thermosensitive polypeptide hydrogels on cartilage repair, Acta Biomater. 73 (2018) 103–111, https://doi.org/10.1016/j.actbio.2018.04.035.
[36] D.P. Walsh, R.D. Murphy, A. Panarella, R.M. Raftery, B. Cavanagh, J.C. Simpson, F. J. O'Brien, A. Heise, S.A. Cryan, Bioinspired star-shaped poly(l-lysine) polypeptides: efficient polymeric nanocarriers for the delivery of DNA to mesenchymal stem cells, Mol. Pharm. 15 (2018) 1878–1891, https://doi.org/10.1021/acs.molpharmaceut.8b00044.
[37] Q. Chen, D. Zhang, W. Zhang, H. Zhang, J. Zou, M. Chen, J. Li, Y. Yuan, R. Liu, Dual mechanism β-amino acid polymers promoting cell adhesion, Nat. Commun. 12 (2021) 562, https://doi.org/10.1038/s41467-020-20858-x.
[38] C. Li, A. Faulkner-Jones, A.R. Dun, J. Jin, P. Chen, Y. Xing, Z. Yang, Z. Li, W. Shu, D. Liu, R.R. Duncan, Rapid formation of a supramolecular polypeptide-DNA hydrogel for in situ three-dimensional multilayer bioprinting, Angew. Chem., Int. Ed. Engl. 54 (2015) 3957–3961, https://doi.org/10.1002/anie.201411383.
[39] D. Zhang, Q. Chen, W. Zhang, H. Liu, J. Wan, Y. Qian, B. Li, S. Tang, Y. Liu, S. Chen, R. Liu, Silk-inspired β-peptide materials resist fouling and the foreign-body response, Angew. Chem., Int. Ed. Engl. 59 (2020) 9586–9593, https://doi.org/10.1002/anie.202000416.
[40] X. Zhou, Z. Li, Advances and biomedical applications of polypeptide hydrogels derived from α-amino acid N-carboxyanhydride (NCA) polymerizations, Adv. Healthc. Mater. 7 (2018), e1800020, https://doi.org/10.1002/adhm.201800020.
[41] M. Zhu, W. Zhong, W. Cao, Q. Zhang, G. Wu, Chondroinductive/chondroconductive peptides and their-functionalized biomaterials for cartilage tissue engineering, Bioact. Mater. 9 (2022) 221–238, https://doi.org/10.1016/j.bioactmat.2021.07.004.
[42] Q. Lv, C. He, F. Quan, S. Yu, X. Chen, DOX/IL-2/IFN-γ co-loaded thermo-sensitive polypeptide hydrogel for efficient melanoma treatment, Bioact. Mater. 3 (2018) 118–128, https://doi.org/10.1016/j.bioactmat.2017.08.003.
[43] C. Zhang, J. Yuan, J. Lu, Y. Hou, W. Xiong, H. Lu, From neutral to zwitterionic poly (α-amino acid) nonfouling surfaces: effects of helical conformation and anchoring orientation, Biomaterials 178 (2018) 728–737, https://doi.org/10.1016/j.biomaterials.2018.01.052.
[44] Y. Hu, Y. Hou, H. Wang, H. Lu, Polysarcosine as an alternative to PEG for therapeutic protein conjugation, Bioconjugate Chem. 29 (2018) 2232–2238, https://doi.org/10.1021/acs.bioconjchem.8b00237.
[45] Y. Hou, Y. Zhou, H. Wang, J. Sun, R. Wang, K. Sheng, J. Yuan, Y. Hu, Y. Chao, Z. Liu, H. Lu, Therapeutic protein PEPylation: the helix of nonfouling synthetic polypeptides minimizes antidrug antibody generation, ACS Cent. Sci. 5 (2019) 229–236, https://doi.org/10.1021/acscentsci.8b00548.
[46] Y. Hou, Y. Zhou, H. Wang, R. Wang, J. Yuan, Y. Hu, K. Sheng, J. Feng, S. Yang, H. Lu, Macrocyclization of interferon-poly(α-amino acid) conjugates significantly improves the tumor retention, penetration, and antitumor efficacy, J. Am. Chem. Soc. 140 (2018) 1170–1178, https://doi.org/10.1021/jacs.7b13017.
[47] Y. Hou, H. Lu, Protein PEPylation: a new paradigm of protein-polymer conjugation, Bioconjugate Chem. 30 (2019) 1604–1616, https://doi.org/10.1021/acs.bioconjchem.9b00236.
[48] Y. Chen, Z. Xu, D. Zhu, X. Tao, Y. Gao, H. Zhu, Z. Mao, J. Ling, Gold nanoparticles coated with polysarcosine brushes to enhance their colloidal stability and circulation time in vivo, J. Colloid Interface Sci. 483 (2016) 201–210, https://doi.org/10.1016/j.jcis.2016.08.038.
[49] W. Viricel, G. Fournet, S. Beaumel, E. Perrial, S. Papot, C. Dumontet, B. Joseph, Monodisperse polysarcosine-based highly-loaded antibody-drug conjugates, Chem. Sci. 10 (2019) 4048–4053, https://doi.org/10.1039/c9sc00285e.

[50] A. Birke, J. Ling, M. Barz, Polysarcosine-containing copolymers: synthesis, characterization, self-assembly, and applications, Prog. Polym. Sci. 81 (2018) 163–208, https://doi.org/10.1016/j.progpolymsci.2018.01.002.

[51] Z. Lu, Y. Wu, Z. Cong, Y. Qian, X. Wu, N. Shao, Z. Qiao, H. Zhang, Y. She, K. Chen, H. Xiang, B. Sun, Q. Yu, Y. Yuan, H. Lin, M. Zhu, R. Liu, Effective and biocompatible antibacterial surfaces via facile synthesis and surface modification of peptide polymers, Bioact. Mater. 6 (2021) 4531–4541, https://doi.org/10.1016/j.bioactmat.2021.05.008.

[52] C.D. Spicer, Hydrogel scaffolds for tissue engineering: the importance of polymer choice, Polym. Chem. 11 (2020) 184–219, https://doi.org/10.1039/c9py01021a.

[53] Z.Y. Tian, Z. Zhang, S. Wang, H. Lu, A moisture-tolerant route to unprotected α/β-amino acid N-carboxyanhydrides and facile synthesis of hyperbranched polypeptides, Nat. Commun. 12 (2021) 5810, https://doi.org/10.1038/s41467-021-25689-y.

[54] M.D. Konieczynska, J.C. Villa-Camacho, C. Ghobril, M. Perez-Viloria, K.M. Tevis, W.A. Blessing, A. Nazarian, E.K. Rodriguez, M.W. Grinstaff, On-demand dissolution of a dendritic hydrogel-based dressing for second-degree burn wounds through thiol-thioester exchange reaction, Angew. Chem., Int. Ed. Engl. 55 (2016) 9984–9987, https://doi.org/10.1002/anie.201604827.

[55] J.J. Hernandez, A.L. Dobson, B.J. Carberry, A.S. Kuenstler, P.K. Shah, K.S. Anseth, T.J. White, C.N. Bowman, Controlled degradation of cast and 3-D printed photocurable thioester networks via thiol–thioester exchange, Macromolecules 55 (2022) 1376–1385, https://doi.org/10.1021/acs.macromol.1c02459.

[56] S.Q. Liu, Q. Tian, L. Wang, J.L. Hedrick, J.H. Hui, Y.Y. Yang, P.L. Ee, Injectable biodegradable poly(ethylene glycol)/RGD peptide hybrid hydrogels for in vitro chondrogenesis of human mesenchymal stem cells, Macromol. Rapid Commun. 31 (2010) 1148–1154, https://doi.org/10.1002/marc.200900818.

[57] M. Yang, Z.C. Zhang, Y. Liu, Y.R. Chen, R.H. Deng, Z.N. Zhang, J.K. Yu, F.Z. Yuan, Function and mechanism of RGD in bone and cartilage tissue engineering, Front. Bioeng. Biotechnol. 9 (2021), 773636, https://doi.org/10.3389/fbioe.2021.773636.

[58] G.I. Im, J.Y. Ko, J.H. Lee, Chondrogenesis of adipose stem cells in a porous polymer scaffold: influence of the pore size, Cell Transplant. 21 (2012) 2397–2405, https://doi.org/10.3727/096368912X638865.

[59] A. Matsiko, J.P. Gleeson, F.J. O'Brien, Scaffold mean pore size influences mesenchymal stem cell chondrogenic differentiation and matrix deposition, Tissue Eng. 21 (2015) 486–497, https://doi.org/10.1089/ten.TEA.2013.0545.

[60] W.L. Fu, C.Y. Zhou, J.K. Yu, A new source of mesenchymal stem cells for articular cartilage repair: MSCs derived from mobilized peripheral blood share similar biological characteristics in vitro and chondrogenesis in vivo as MSCs from bone marrow in a rabbit model, Am. J. Sports Med. 42 (2014) 592–601, https://doi.org/10.1177/0363546513512778.

[61] Y.R. Chen, X. Yan, F.Z. Yuan, J. Ye, B.B. Xu, Z.X. Zhou, Z.M. Mao, J. Guan, Y. F. Song, Z.W. Sun, X.J. Wang, Z.Y. Chen, D.Y. Wang, B.S. Fan, M. Yang, S.T. Song, D. Jiang, J.K. Yu, The use of peripheral blood-derived stem cells for cartilage repair and regeneration in vivo: a review, Front. Pharmacol. 11 (2020) 404, https://doi.org/10.3389/fphar.2020.00404.

[62] J.L. Cook, C.T. Hung, K. Kuroki, A.M. Stoker, C.R. Cook, F.M. Pfeiffer, S. L. Sherman, J.P. Stannard, Animal models of cartilage repair, Bone Joint Res. 3 (2014) 89–94, https://doi.org/10.1302/2046-3758.34.2000238.

[63] H. Kang, B. Yang, K. Zhang, Q. Pan, W. Yuan, G. Li, L. Bian, Immunoregulation of macrophages by dynamic ligand presentation via ligand-cation coordination, Nat. Commun. 10 (2019) 1696, https://doi.org/10.1038/s41467-019-09733-6.

[64] G. Jiang, S. Li, K. Yu, B. He, J. Hong, T. Xu, J. Meng, C. Ye, Y. Chen, Z. Shi, G. Feng, W. Chen, S. Yan, Y. He, R. Yan, A 3D-printed PRP-GelMA hydrogel promotes osteochondral regeneration through M2 macrophage polarization in a rabbit model, Acta Biomater. 128 (2021) 150–162, https://doi.org/10.1016/j.actbio.2021.04.010.

[65] H. Zhang, D. Cai, X. Bai, Macrophages regulate the progression of osteoarthritis, Osteoarthritis Cartilage 28 (2020) 555–561, https://doi.org/10.1016/j.joca.2020.01.007.